Original Article

Usefulness of attenuation value on computed tomography plain scan for diagnosing enlarged mediastinal lymph nodes metastases

Zhi-Long Wang[1#^], Yan Yan[2#], Xiao-Ting Li[1], Yan-Ling Li[1], Zhong-Wu Li[3], Ying-Shi Sun[1^]

[1]Key Laboratory of Carcinogenesis and Translational Research (Ministry of Education/Beijing), Department of Radiology, Peking University Cancer Hospital and Institute, Beijing, China; [2]Key Laboratory of Carcinogenesis and Translational Research (Ministry of Education/Beijing), Endoscopy Center, Peking University Cancer Hospital and Institute, Beijing, China; [3]Key Laboratory of Carcinogenesis and Translational Research (Ministry of Education/Beijing), Department of Pathology, Peking University Cancer Hospital and Institute, Beijing, China

Contributions: (I) Conception and design: ZL Wang, Y Yan; (II) Administrative support: YS Sun; (III) Provision of study materials or patients: ZL Wang, Y Yan; (IV) Collection and assembly of data: ZL Wang, Y Yan, ZW Li; (V) Data analysis and interpretation: ZL Wang, YL Li, XT Li; (VI) Manuscript writing: All authors; (VII) Final approval of manuscript: All authors.

[#]These authors contributed equally to this work and should be considered as co-first authors.

Correspondence to: Ying-Shi Sun, MD. Key Laboratory of Carcinogenesis and Translational Research (Ministry of Education/Beijing), Department of Radiology, Peking University Cancer Hospital and Institute, 52 Fucheng Road, Haidian District, Beijing 100142, China. Email: sys27@163.com.

Background: To evaluate the diagnostic value of computed tomography (CT) attenuation in mediastinal lymph node metastases of malignant tumors.

Methods: A retrospective review was conducted of a Chinese institutional database of consecutive patients with a history of malignant tumors. Those who had enlarged, necrotic, or hypermetabolic lymph nodes detected in the mediastinum during routine CT examination or positron emission tomography (PET)/CT imaging from January 2019 to December 2021 were collected for investigation. All patients underwent endobronchial ultrasound-guided transbronchial needle aspiration (EBUS-TBNA) and were followed up for at least 6 months to diagnose lymph node metastases. One-to-one correlation was attempted between the CT images of the lymph nodes and EBUS-TBNA area of the same lymph node groups and similar size. Radiologists measured size, as well as plain CT and contrast-enhanced CT (CECT) attenuation values of mediastinal lymph nodes, and evaluated the effectiveness of these variables in diagnosing lymph node metastasis.

Results: A total of 135 lymph nodes of 114 patients were included in the study. In the univariate analysis, the long-axis diameter, short-axis diameter, short-axis/long-axis ratio, and plain CT attenuation values of lymph nodes were found to be statistically significantly different between the metastatic and non-metastatic lymph nodes. The areas under receiver operator characteristic (ROC) curves (AUCs) of long-axis diameter, short-axis diameter, short-axis/long-axis ratio, and plain CT attenuation value for diagnosing metastases were 0.711, 0.788, 0.671, and 0.827, respectively. The best value of the AUC for diagnosing lymph node metastases was 0.827 [95% confidence interval (CI): 0.749–0.890] using plain CT attenuation value ≤45 Hounsfield units (HU). The sensitivity, specificity, positive predictive value (PPV), and negative predictive value (NPV) were 92.8%, 69.2%, 86.5%, and 81.8%, respectively. Similar results were obtained from the 68 cases of lung cancer. Plain CT attenuation values reached the best AUC (0.860) for diagnosing lymph node metastases.

^ ORCID: Zhi-Long Wang, 0000-0002-0268-8246; Ying-Shi Sun, 0000-0001-9424-1910.

Conclusions: Plain CT attenuation of lymph nodes is an effective method for diagnosing enlarged mediastinal lymph nodes with a history of multiple malignancies or lung cancer. Plain CT could be used as an additional test where there is no PET/CT available in cases of diagnostic dilemma.

Keywords: Mediastinum; lymph node metastases; computed tomography attenuation; malignancy

Submitted Nov 24, 2022. Accepted for publication Jun 19, 2023. Published online Jul 18, 2023.
doi: 10.21037/qims-22-1305
View this article at: https://dx.doi.org/10.21037/qims-22-1305

Introduction

Chest computed tomography (CT) is a less invasive imaging method that is routinely used to detect mediastinal lymph node metastases in the initial staging or therapeutic follow-up of malignant tumors. Regarding the screening protocol for many malignant tumors after radical treatment, the National Comprehensive Cancer Network (NCCN) guidelines recommend that plain and/or enhanced CT scans should be conducted every 3–6 months for surveillance. Metastases are suspected when mediastinal lymph nodes are enlarged or necrotic. Currently, the most commonly used CT-based diagnostic criterion for mediastinal lymph node metastases is a mediastinal lymph node diameter >10 mm (1,2). However, several studies have shown that CT does not accurately identify pathological mediastinal lymphadenopathy (sensitivity, 51–64%; specificity, 74–86%) (3,4). Abnormal shape or attenuation of the lymph nodes can also be a sign of metastatic involvement. The presence of central low-attenuation areas indicates necrosis and increases the specificity of CT for the diagnosis of metastases (3). At present, there is no clear standard of CT attenuation for diagnosing mediastinal lymph node metastases. The present study aimed to evaluate the diagnostic value of CT attenuation in mediastinal lymph node metastases of malignant tumors. We present this article in accordance with the Standards for Reporting Diagnostic Accuracy Studies (STARD) reporting checklist (available at https://qims.amegroups.com/article/view/10.21037/qims-22-1305/rc).

Methods

Participants

This retrospective study was approved by the institutional review board of Peking University Cancer Hospital and Institute, and conducted according to the guidelines of the Declaration of Helsinki (as revised in 2013). The requirement for informed consent was waived given the retrospective nature of the study. A total of 137 consecutive patients with a history of malignant tumors who were diagnosed with enlarged or necrotic lymph nodes in the mediastinum on routine CT reports or hypermetabolic nodes on positron emission tomography (PET)/CT scans [maximum standardized uptake value (SUVmax) ≥2.5] from January 2019 to December 2021 were enrolled in the study. To make a definitive diagnosis of these suspected enlarged lymph nodes, all patients underwent endobronchial ultrasound-guided transbronchial needle aspiration (EBUS-TBNA) and were followed-up for at least 6 months. The pathological results of EBUS-TBNA were used to diagnose lymph node metastases. Patients who underwent CT examinations in other hospitals were excluded. A diagram showing the detailed inclusion/exclusion criteria is displayed in *Figure 1*. Since the endoscopy doctor had reviewed the location of the target lymph nodes on CT images before EBUS-TBNA, a one-to-one correlation was performed between CT images of the lymph nodes and the EBUS-TBNA area by the same groups of lymph nodes and similar sizes. Radiologists measured the size, as well as the plain and contrast-enhanced CT (CECT) attenuation values of mediastinal lymph nodes.

EBUS-TBNA procedure

A bronchoscope (BF-UC260F-OL8, Olympus, Tokyo, Japan; EB-530US, Fujifilm, Tokyo, Japan) was used to operate the EBUS-TBNA. Pre-operation preparation included ensuring that the stomach was empty and the provision of topical anesthesia. The bronchoscope was inserted into the trachea and bronchial tree through the nostrils or mouth. After identifying the targeted lymph nodes, ultrasound images were saved and the features were described. Biopsy was performed via 1–3 punctures with a 22- or 25-gauge needle to obtain sufficient samples.

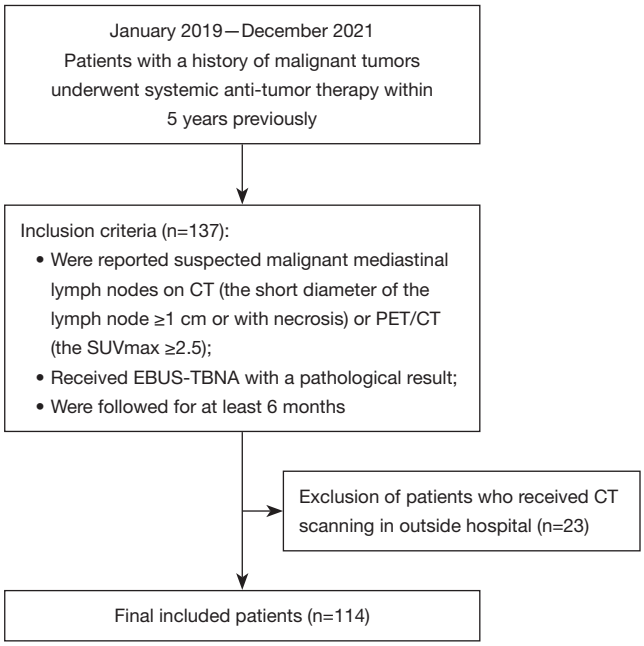

Figure 1 The flowchart of the study. CT, computed tomography; PET, positron emission tomography; SUVmax, maximum standardized uptake; EBUS-TBNA, endobronchial ultrasound-guided transbronchial needle aspiration.

Pathological examinations were performed to determine the presence of malignant cells in the biopsy tissue. The CT results were not made available to the assessors of EBUS-TBNA pathological results.

CT protocol

A CT scanner with 64 rows of detectors (LightSpeed 64; GE Healthcare, Milwaukee, WI, USA) was used to perform the chest CT scans. Plain CT scan was carried out from apex pulmonis to the diaphragm dome (collimation: 0.625 mm, peak tube voltage: 120 kVp, tube current-time product: automatic). Next, 80 mL of a non-ionic contrast medium (Ultravist 300 mg/mL; Bayer, Munich, Germany) was administered intravenously at a rate of 3 mL/s with an automatic injector. The contrast-enhanced scan began 40 seconds after injection of the contrast medium.

Image analysis

Image analysis was performed independently by two radiologists with 13 and 12 years of experience in chest imaging using the workstation (Carestream Health Inc., Shanghai, China). They reviewed the CT images of the mediastinum to detect lymph nodes with long-axis diameter ≥10 mm. Then, the radiologists carried out a one-to-one correlation between CT images of lymph nodes and the EBUS-TBNA area of the same lymph node groups and similar sizes. They were blinded to the pathological results of the lymph nodes. When they had completed the one-to-one correlation and confirmed the locations of the target lymph nodes, image measurements including long- and short-axis diameters of the lymph nodes on axial CT images, plain CT attenuation values of the lymph nodes, and enhanced CT attenuation values of lymph nodes were recorded for statistical analysis. These two radiologists independently drew a round region of interest (ROI) as large as possible within each lymph node. The ROI was placed in the slice in which the lymph node showed the largest area on the axial CT image. CT attenuation measurement was performed to exclude calcification, vessels, or artifacts within the ROI. The measured CT values were the average values of the ROIs. After the assessment of interobserver agreement, the image measurement data of the first radiologist were used for statistical analysis.

Statistical analysis

Data processing and data analysis were performed using the software SPSS 22.0 (IBM Corp., Armonk, NY, USA). Long-axis diameter, short-axis diameter, short-axis/long-axis ratio, plain CT attenuation values of lymph nodes, and CECT attenuation values of lymph nodes were compared using the independent-samples *t*-test and binary logistic regression. These measurement variables were treated as continuous measurement data. Correlation analysis was conducted and Pearson's r was calculated. When a Pearson's r larger than 0.60 was observed, the feature with the smaller P value in the independent-samples *t*-test would be introduced into the binary logistic regression, whereas the feature with the larger P value would not. The interaction analysis was carried out between CT signs and multiple malignancies (lung cancer/non-lung cancer) using a logistic regression model to explore the possible heterogeneity. If the interaction P value was >0.1, heterogeneity was not considered. The area under the receiver operating characteristic (ROC) curves (AUCs) of the above-mentioned CT features, sensitivity, specificity, positive predictive value (PPV), and negative predictive value (NPV) were calculated to evaluate the diagnostic capability for lymph node metastases. The optimal cut-off value was selected when we

Table 1 Baseline demographics and clinical characteristics of the patients

Patient or LN characteristics	Study sample
No. of patients	114
Age (year), median [range]	60 [28–77]
Sex	
Male	72
Female	42
Frequency of biopsied LN stations	
4R	54
4L	15
7	40
10-11R	20
10-11L	5
Others	1

LN, lymph node.

obtained the largest Youden index (sensitivity + specificity − 1). The interobserver agreement of the quantitative data was evaluated by Bland–Altman analysis. Statistical significance was considered when P<0.05.

For the 68 patients with lung cancer, who comprised the bulk of our research population, we also performed the univariate analysis and logistic regression to compare long-axis diameter, short-axis diameter, plain CT attenuation values, and CECT attenuation values between the malignant and benign lymph nodes. ROC curves were used to evaluate the diagnostic power for lymph node metastases for these CT features which had statistical significance in univariate analysis.

Results

Patient characteristics

After excluding 23 patients who had undergone CT examinations in other hospitals, 114 patients (male, n=72; female, n=42; median age, 60 years; range of age, 28–77 years) with complete clinical and CT data were involved in the study (*Table 1*). Regarding the primary tumor of these patients, there were 68 patients with lung cancer, 21 patients with renal cancer, 5 patients with carcinoma of the uterine cervix, 4 patients with head-neck carcinoma, 2 patients with liver carcinoma, 2 patients with gastric cancer, 5 patients with colorectal cancer, 1 patient with prostatic carcinoma, 1 patient with thymic carcinoma, 4 patients with neuroendocrine carcinoma, and 1 patient with olfactory neuroblastoma. Among 135 lymph nodes of 114 patients, 92 lymph nodes were malignant and 43 nodes were benign. All benign nodes were reactive nodes on pathology. The median distance between CT and EBUS was 2 weeks (range, 10–16 days).

Image analysis

A total of 135 lymph nodes were detected by the researchers. In addition, 91 patients underwent both plain and CECT scans; 12 patients underwent plain CT scan only; 11 patients received CECT scan only. Some 18 lymph nodes in 15 cases were hypermetabolic (SUVmax ≥2.5). The results of the Bland-Altman analysis revealed that the long-axis diameter, short-axis diameter, and plain CT attenuation reached interobserver agreement (P>0.05) (*Figure 2*). The ranges of long-axis diameter, short-axis diameter, and plain CT attenuation were 8–82 mm, 5–62 mm, and 10–79 HU, respectively. The long-axis diameter of metastatic lymph nodes (mean ± SD, 27.01±12.21 mm) was larger than that of non-metastatic lymph nodes (19.65±6.68 mm) (P<0.001). The short-axis diameter of metastatic lymph nodes (18.78±8.88 mm) was larger than that of non-metastatic lymph nodes (11.47±3.96 mm) (P<0.001). The short-axis/long-axis diameter ratio of metastatic lymph nodes (0.70±0.13) was larger than that of non-metastatic lymph nodes (0.60±0.14) (P<0.001). The plain CT attenuation value of metastatic lymph nodes (35.99±10.16 HU) was lower than that of non-metastatic lymph nodes (49.71±13.09 HU) (P<0.001). The CECT attenuation value of lymph nodes was not significantly different between the benign and malignant lymph nodes (P=0.153) (*Table 2*). On account of a strong correlation detected between the long and short diameters in the Pearson correlation analysis (Pearson's r =0.893), long-axis diameter was excluded from the logistic regression (Table S1). In the binary logistic regression analysis, short-axis diameter and plain CT attenuation were the independent predictors of malignant lymph nodes (*Table 2*). The AUCs of long-axis diameter, short-axis diameter, short-axis/long-axis ratio, and plain CT attenuation value for diagnosing metastases were 0.711 [95% confidence interval (CI): 0.622–0.789], 0.788 (95% CI: 0.705–0.857), 0.671 (95% CI: 0.580–0.753), and 0.827 (95% CI: 0.749–0.890), respectively (*Figure 3A*). When the plain CT attenuation

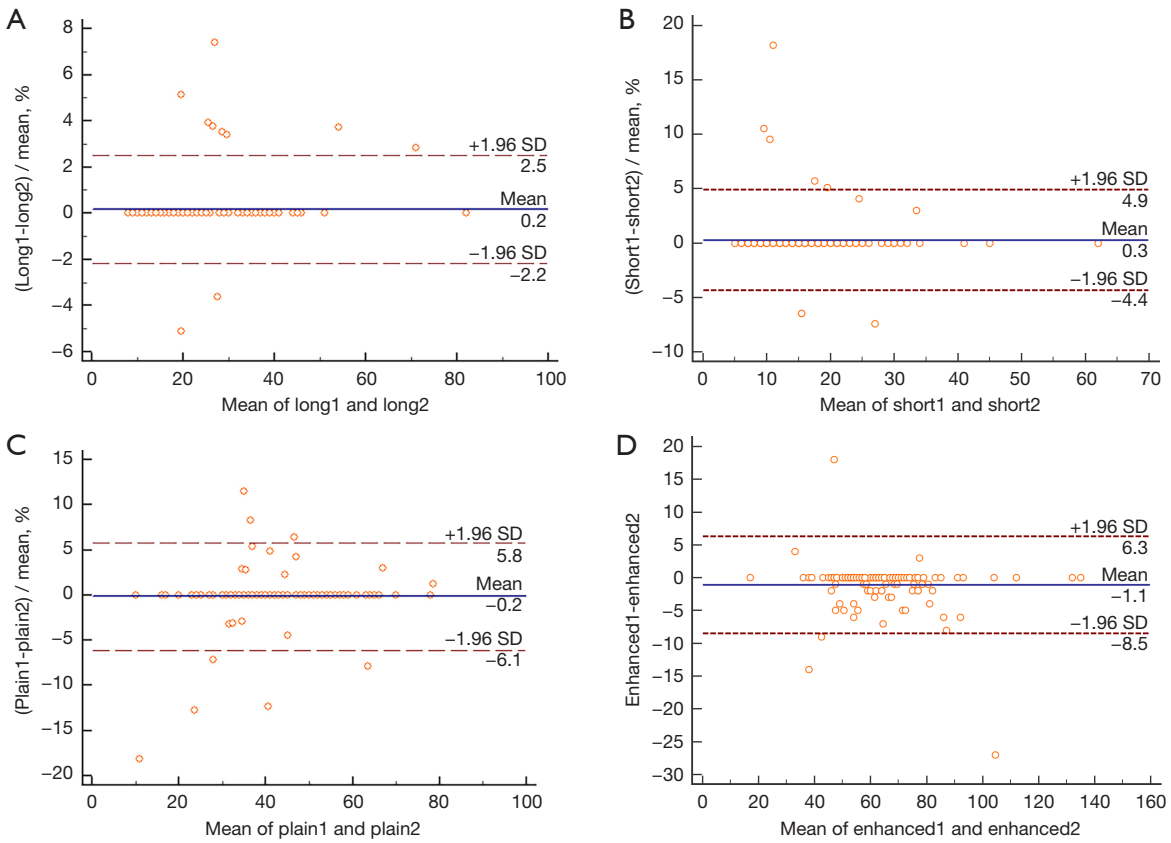

Figure 2 The results of Bland-Altman analysis. (A-D) The results of the Bland-Altman analysis revealed that the long-axis diameter, short-axis diameter, and plain CT attenuation of 2 observers reached an interobserver agreement (P>0.05). (A-C) The P value was 0.07, 0.193, and 0.57, respectively. (D) The enhanced CT attenuation of the 2 observers did not reach an interobserver agreement (P=0.002). SD, standard deviation; CT, computed tomography.

Table 2 Comparison of CT imaging features between malignant lymph nodes and benign lymph nodes

CT imaging features	Malignant lymph nodes	Benign lymph nodes	Univariate analysis	Binary logistic regression	
			P value	P value	OR (95% CI)
Long-axis diameter (mm)	27.01±12.21 [8–82]	19.65±6.68 [9–41]	<0.001	N/A	N/A
Short-axis diameter (mm)	18.78±8.88 [6–62]	11.47±3.96 [5–24]	<0.001	0.001	1.199 (1.076–1.337)
Short-axis/long-axis ratio	0.70±0.13 [0.34–1.00]	0.60±0.14 [0.36–0.92]	<0.001	0.215	13.743 (0.218–865.97)
Plain CT attenuation (HU)	35.99±10.16 [10–79]	49.71±13.09 [10–70]	<0.001	<0.001	0.901 (0.854–0.951)
Contrast-enhanced CT attenuation (HU)	62.23±18.84 [17–135]	67.36±17.06 [31–121]	0.153	0.449	1.013 (0.98–1.048)

Data are shown as mean ± SD [range]. CT, computed tomography; OR, odds ratio; CI, confidence interval; HU, Hounsfield unit; N/A, not applicable; SD, standard deviation.

value ≤45 HU was regarded as the diagnostic criterion for lymph node metastases, the sensitivity, specificity, PPV, and NPV were 92.8%, 69.2%, 86.5%, and 81.8%, respectively (*Table 3*).

In the 76 lymph nodes of 68 patients with lung cancer, the long-axis diameter, short-axis diameter, plain CT attenuation values, and CECT attenuation values all had statistically significant differences between metastatic lymph

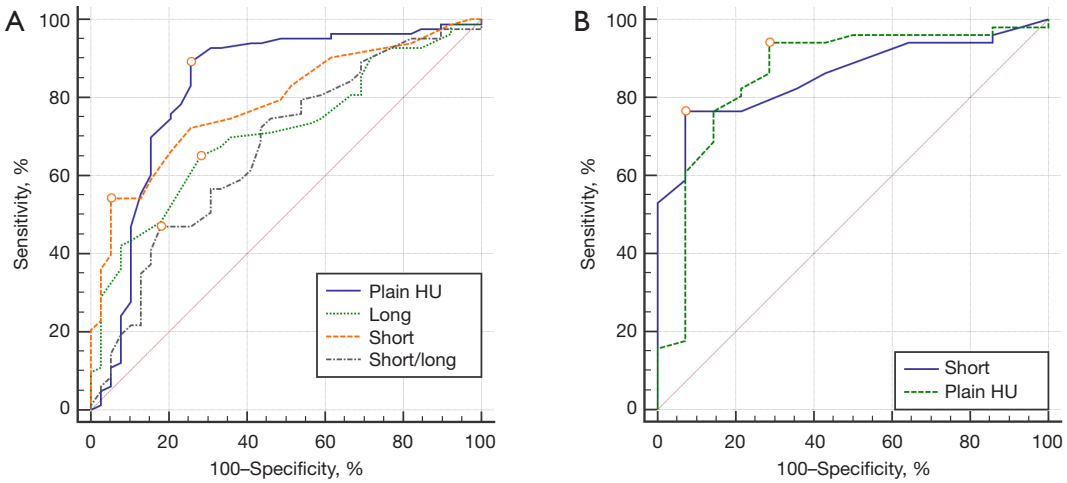

Figure 3 The ROC curves of CT features for diagnosing the enlarged malignant lymph nodes in all cases and lung cancer. (A) The ROC curves of CT features for diagnosing the enlarged malignant lymph nodes in all cases. Plain CT attenuation achieved the best diagnostic capability (AUC =0.827, 95% CI: 0.749–0.890). (B) In the 68 cases of lung cancer, plain CT attenuation achieved the best AUC (0.860, 95% CI: 0.751–0.934) on the ROC curve. HU, Hounsfield unit; ROC, receiver operating characteristic curve; CT, computed tomography; AUC, area under receiver operating characteristic curve; CI, confidence interval.

Table 3 The diagnostic capability of CT features for enlarged malignant lymph nodes by ROC curves

CT features	Best cutoff	Sensitivity (%)	Specificity (%)	PPV (%)	NPV (%)	AUC	P value
Long-axis diameter	>23 mm	61.7	73.2	84.1	45.5	0.711	<0.001
Short-axis diameter	>13 mm	72.3	75.6	87.2	54.4	0.788	<0.001
Short-axis/long-axis ratio	>0.6	74.5	56.1	79.5	48.5	0.671	0.001
Plain CT attenuation	≤45 HU	92.8	69.2	86.5	81.8	0.827	<0.001

CT, computed tomography; ROC, receiver operating characteristic curve; PPV, positive predictive value; NPV, negative predictive value, AUC, area under the ROC curve.

Table 4 Comparison of CT imaging features between malignant lymph nodes and benign lymph nodes in 68 cases of lung cancer

CT imaging features	Malignant lymph nodes	Benign lymph nodes	Univariate analysis	Binary logistic regression	
			P value	P value	OR (95% CI)
Long-axis diameter (mm)	26.75±11.01	17.88±5.29	0.003	0.356	1.111 (0.889–1.388)
Short-axis diameter (mm)	18.70±8.66	10.13±2.68	<0.001	0.033	0.614 (0.392–0.961)
Plain CT attenuation (HU)	34.55±11.33	50.50±12.29	<0.001	0.028	1.091 (1.009–1.180)
Contrast-enhanced CT attenuation (HU)	60.09±13.16	70.20±15.66	0.013	0.807	0.991 (0.919–1.068)

Data are shown as mean ± SD. CT, computed tomography; OR, odds ratio; CI, confidence interval; HU, Hounsfield unit; SD, standard deviation.

nodes and non-metastatic lymph nodes (P<0.05) (*Table 4*). In the logistic regression analysis, short-axis diameter and plain CT attenuation were the independent predictors of malignant lymph nodes (P<0.05). The interaction P values between multiple malignancies (lung cancer/non-lung cancer) and CT signs (short axis diameter and plain CT attention) were both larger than 0.999. The AUCs of short-axis diameter and plain CT attenuation value for diagnosing

Table 5 The diagnostic capability of CT features for enlarged malignant lymph nodes in 68 cases of lung cancer by ROC curves

CT features	Best cutoff	Sensitivity (%)	Specificity (%)	PPV (%)	NPV (%)	AUC	P value
Short-axis diameter	>13 mm	75.0	93.8	97.8	50.0	0.858	<0.001
Plain CT attenuation	≤45 HU	94.1	71.4	92.3	76.9	0.860	<0.001

CT, computed tomography; ROC, receiver operating characteristic; PPV, positive predictive value; NPV, negative predictive value; AUC, area under the ROC curve; HU, Hounsfield unit.

metastases were 0.858 (95% CI: 0.749–0.932) and 0.860 (95% CI: 0.751–0.934), respectively (*Figure 3B*, *Table 5*).

Discussion

Mediastinal lymph node metastases are very important in the initial staging of malignant tumors, and can be regarded as a valuable prognostic factor. Furthermore, when mediastinal lymphadenopathy occurs in the course of tumor treatment, the diagnosis of lymph node metastasis plays a key role in determining the ongoing treatment strategy. Invasive diagnostic methods, including video-assisted thoracoscopic surgery and EBUS-TBNA, can diagnose mediastinal lymph node metastases accurately (5-7). Some non-invasive imaging techniques, such as enhanced CT and ^{18}F-fluorodeoxyglucose (^{18}F-FDG) PET, are also commonly utilized for diagnosing metastatic lymph nodes in patients with lung cancer, esophageal cancer, or other malignances. However, the precision of conventional CT features in the diagnosis of lymph node metastases in patients with lung cancer is approximately 60% (8,9). Diagnostic imaging methods that use size as the criterion of nodal infiltration cannot accurately assess the nodal status of patients with esophageal carcinoma (10,11). Recently, Nagano *et al.* reported that electron density of dual-energy CT may be useful for diagnosing metastatic lymph nodes in non-small cell lung cancer. The accuracy was highest for the combination of electron density and short-axis diameter (accuracy, 82.9%; sensitivity, 54.5%; specificity, 94.0%) and the combination of electron density and false positive FDG uptake (accuracy, 82.1%; sensitivity, 60.6%; specificity, 90.5%) (12). However, the sensitivity is still insufficient to detect mediastinal lymph node metastases.

Metastatic lymph nodes are frequently diagnosed in clinical processes by the size-dependent criterion (1,2,9,13). However, the detection of small metastatic lymph nodes using CT features is a diagnostic challenge (10). In this present study, we concentrated on the lymph nodes with a long-axis diameter >10 mm, which were considered suspicious of metastases by CT and PET/CT. For these enlarged lymph nodes, our results showed that the long- and short-axis diameters were both significantly different between the metastatic and non-metastatic lymph nodes. Short-axis diameter achieved a higher AUC (0.788) for diagnosing metastases than long-axis diameter (0.711) (P<0.001). Different from the conventional criterion of maximum short-axis diameter ≥10 mm, the cutoff value of short-axis diameter in our study was 13 mm, which achieved a sensitivity of 72.3% and a specificity of 75.6%. Short-axis/long-axis diameter ratio can be valuable in the diagnosis of metastatic lymph nodes in patients with lung cancer or gastric cancer (12,14). However, the AUC of short-axis/long-axis diameter ratio (0.671) was relatively lower than that of short-axis diameter (0.788) in our study.

The main finding of our study was that the plain CT attenuation of lymph nodes could be valuable for diagnosing metastases, achieving the best AUC (0.827). Metastatic lymph node HU values were lower, and HU values of benign lymph nodes were higher (*Figures 4-6*). Some studies have found that the necrosis was obviously more prevalent in metastatic lymph nodes than in non-metastatic lymph nodes (15,16). Necrosis causes a reduction in the density of lymph nodes. This was one possible interpretation for our results, in which metastatic lymph nodes had lower plain CT attenuation values. However, the CECT attenuation values of lymph nodes were not significantly different between the metastatic and non-metastatic lymph nodes in our study. This could be related to the fact that necrosis of lymph nodes is mainly associated with a low CECT attenuation value, especially in the delayed phase (12). Therefore, necrosis was not the only reason for the difference in the CT attenuation values of metastatic lymph nodes in our study. Thoracic lymph node enlargement can be found in several benign diseases, such as tuberculosis, granulomatous, sarcoidosis, anthracosis, and pneumoconiosis (15,17-19). Furthermore, enlarged mediastinal lymph nodes can be detected in up to 52% of heavy smokers, or in patients with chronic obstructive

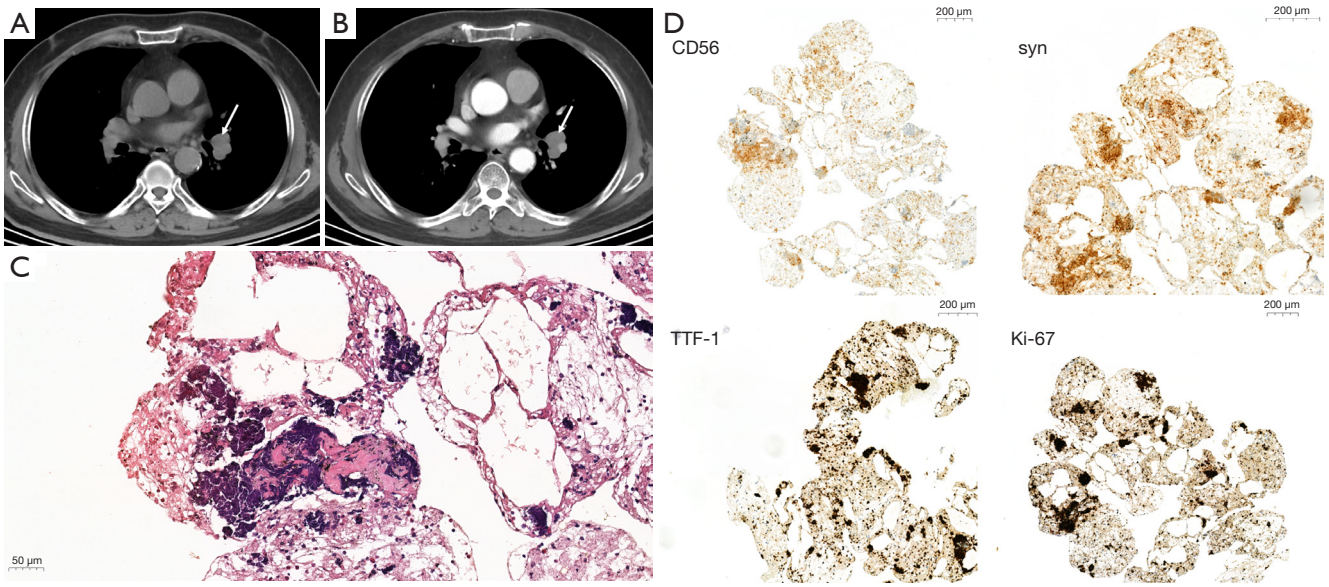

Figure 4 A case of malignant node with small cell lung cancer in one patient of esophageal squamous carcinoma. (A-D) A 59-year-old male patient with esophageal squamous carcinoma. Chest CT detected an enlarged lymph node at 10L group (white arrows). The pathological results of EBUS-TBNA indicated small cell lung cancer. The size of this lymph node was 18 mm × 14 mm. (A) The plain CT attenuation value was 19 HU. (B) The CECT attenuation value was 51 HU. (C,D) The photomicrograph of pathological specimen showed poorly differentiated tumor cells within fibrinous exudate. The cells had less cytoplasm, hyperchromatic nuclei, and extrusion appearance (hematoxylin-eosin stain; original magnification, ×200). Combined with immunohistochemistry (CD56, TTF-1, syn, Ki-67), the lymph node was diagnosed as metastasis of small cell lung carcinoma. CT, computed tomography; EBUS-TBNA, endobronchial ultrasound-guided transbronchial needle aspiration; mm, millimeter; HU, Hounsfield unit; CECT, contrast-enhanced CT; CD56, cluster designation 56; TTF-1, thyroid transcription factor-1; syn, synaptophysin; Ki-67, proliferation index.

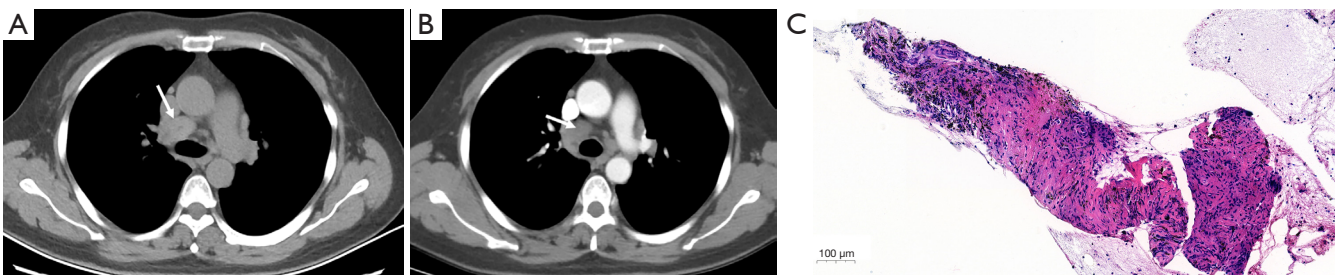

Figure 5 A benign mediastinal lymph node of a patient with carcinoma of uterine cervix. (A-C) A 51-year-old female patient with carcinoma of the uterine cervix. The pathological results of EBUS-TBNA indicated a benign lymph node. Chest CT detected an enlarged lymph node at 4R group of the mediastinum (white arrows). The size of this lymph node was 18 mm × 14 mm. (A) The plain CT attenuation value was 55 HU. (B) The CECT attenuation value was 60 HU. (C) The photomicrograph of pathological specimen showed the inflammatory cell infiltration and no malignancy in this lymph node (hematoxylin-eosin staining; original magnification, ×100). EBUS-TBNA, endobronchial ultrasound-guided transbronchial needle aspiration; mm, millimeter; CT, computed tomography; HU, Hounsfield unit; CECT, contrast-enhanced CT.

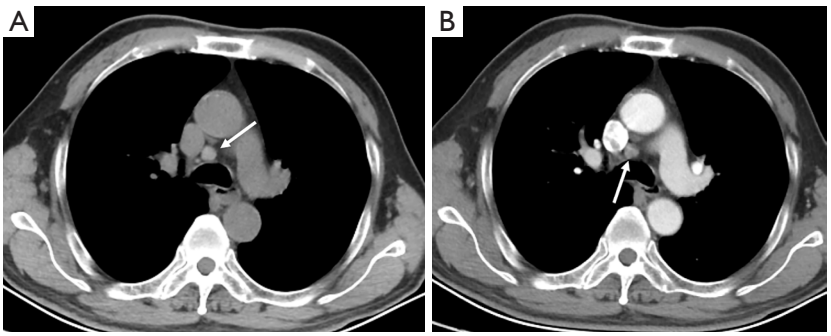

Figure 6 A non-metastatic node in a patient with gastric carcinoma. (A,B) A 70-year-old male patient with gastric carcinoma and pathologically confirmed non-metastatic node. Chest CT detected an enlarged lymph node at 4R group (white arrows). The pathological results of EBUS-TBNA indicated benign lymph node. The size of this lymph node was 10 mm × 10 mm. (A) The plain CT attenuation value was 62 HU. (B) The CECT attenuation value was 65 HU. CT, computed tomography; EBUS-TBNA, endobronchial ultrasound-guided transbronchial needle aspiration; CECT, contrast-enhanced CT; HU, Hounsfield unit.

pulmonary disease (20). Calcification and deposition of anthracotic pigment have been occasionally observed in enlarged lymph nodes in these benign proliferative diseases (21,22). Calcification and anthracotic pigment may increase the plain CT attenuation values of lymph nodes. Calcification is not an absolutely specific sign for the diagnosis of benign lymph nodes. Spotty or indistinct calcification may also be occasionally observed in metastatic lymph nodes, especially in metastases of colon and breast cancers. Bayanati *et al.* reported opposite results by comparing 34 malignant lymph nodes and 41 benign lymph nodes (23). They found that the mean CT attenuation value was 22±16 HU for benign lymph nodes and 29±13 HU for malignant lymph nodes (P=0.04). However, the range of lymph nodes size was different from our findings. In our study, benign lymph nodes varied in size from 3 to 14 mm in short-axis diameter (mean size, 7.4±2.9 mm), whereas all benign lymph nodes in Bayanati *et al.*'s study were normal or reactive nodes on pathology. Those normal small lymph nodes (<10 mm) may contain fat density, which may reduce the CT attenuation value. A prospective, multicenter, large-scale study is required to verify the diagnostic capability of plain CT attenuation for malignant lymph nodes.

Our results showed that the plain CT attenuation value ≤45 HU could be considered as the diagnostic criterion for malignant lymph nodes. The PPV and NPV reached 86.5% and 81.8%, respectively, in this study. The PPV and NPV results are not sufficient to alter treatment decisions; the pathological findings of the lymph nodes are still needed to guide treatment strategies. For patients suspected of positive metastases on plain CT examination, we recommend biopsy to obtain pathological confirmation. Doing so would enable these patients to receive the anti-tumor therapy in time. For patients diagnosed as negative for metastases on plain CT scan, oncologists may offer the choice of a short-term follow-up CT scan. If the lymph nodes remain stable during follow-up, this approach may circumvent potential injury to the patient from an invasive biopsy.

Our study had some limitations. First, in population selection, we included different types of tumors. The number of mediastinal nodes was relatively small for a large number of different tumor types. Due to the relatively small sample sizes, our results may have been influenced by sampling bias. Second, this was a retrospective study. Although the data were collected from more than 100 cases, the conclusions still need to be further confirmed by large-scale, prospective, multicenter studies. Third, we used the pathological results of EBUS-TBNA as the standard to diagnose lymph node metastases. Although the accuracy of EBUS-TBNA for diagnosing metastatic nodes was quite high (approximately 90%), it was slightly different from the results of surgery. In our study, patients were followed up for at least 6 months to confirm the status of lymph nodes. Fourth, we only analyzed the CT values of lymph nodes with a single enhanced phase (delay time 40 s). We will proceed to collect multi-phase CT cases to further investigate the ability of post contrast attenuation to diagnose lymph node metastasis in the future study.

Conclusions

Plain CT attenuation value of the lymph node was found to

be more effective than the lymph node size in diagnosing enlarged mediastinal lymph nodes with a history of malignancy. Plain CT could be used as a problem-solving technique in cases where there is no PET/CT available, and/or the patients do not want to undergo EBUS-TBNA. In some other institutions where the plain CT is not routinely performed, plain CT could be used as an additional test in cases of diagnostic dilemma for suspicious mediastinal lymph nodes.

Acknowledgments

We thank Kun Cao, Lei Tang, Yong Cui, and Shun-Yu Gao for editorial support and Xiao-Yan Zhang and Li-Ping Qi for reviewing the manuscript. The affiliation of them is the Department of Radiology, Peking University Cancer Hospital & Institute, Beijing, China.
Funding: This study was supported by Beijing Hospitals Authority'Ascent Plan (No. DFL20191103).

Footnote

Reporting Checklist: The authors have completed the STARD reporting checklist. Available at https://qims.amegroups.com/article/view/10.21037/qims-22-1305/rc

Conflicts of Interest: All authors have completed the ICMJE uniform disclosure form (available at https://qims.amegroups.com/article/view/10.21037/qims-22-1305/coif). The authors have no conflicts of interest to declare.

Ethical Statement: The authors are accountable for all aspects of the work in ensuring that questions related to the accuracy or integrity of any part of the work are appropriately investigated and resolved. The retrospective study was approved by the institutional review board of Peking University Cancer Hospital and Institute, and conducted according to the guidelines of the Declaration of Helsinki (as revised in 2013). The requirement for informed consent was waived given the nature of the retrospective study.

References

1. Seely JM, Mayo JR, Miller RR, Müller NL. T1 lung cancer: prevalence of mediastinal nodal metastases and diagnostic accuracy of CT. Radiology 1993;186:129-32.
2. Gross BH, Glazer GM, Orringer MB, Spizarny DL, Flint A. Bronchogenic carcinoma metastatic to normal-sized lymph nodes: frequency and significance. Radiology 1988;166:71-4.
3. Walker CM, Chung JH, Abbott GF, Little BP, El-Sherief AH, Shepard JA, Lanuti M. Mediastinal lymph node staging: from noninvasive to surgical. AJR Am J Roentgenol 2012;199:W54-64.
4. Silvestri GA, Gould MK, Margolis ML, Tanoue LT, McCrory D, Toloza E, Detterbeck F; . Noninvasive staging of non-small cell lung cancer: ACCP evidenced-based clinical practice guidelines (2nd edition). Chest 2007;132:178S-201S.
5. Ernst A, Anantham D, Eberhardt R, Krasnik M, Herth FJ. Diagnosis of mediastinal adenopathy-real-time endobronchial ultrasound guided needle aspiration versus mediastinoscopy. J Thorac Oncol 2008;3:577-82.
6. Annema JT, van Meerbeeck JP, Rintoul RC, Dooms C, Deschepper E, Dekkers OM, De Leyn P, Braun J, Carroll NR, Praet M, de Ryck F, Vansteenkiste J, Vermassen F, Versteegh MI, Veseliç M, Nicholson AG, Rabe KF, Tournoy KG. Mediastinoscopy vs endosonography for mediastinal nodal staging of lung cancer: a randomized trial. JAMA 2010;304:2245-52.
7. Yasufuku K, Pierre A, Darling G, de Perrot M, Waddell T, Johnston M, da Cunha Santos G, Geddie W, Boerner S, Le LW, Keshavjee S. A prospective controlled trial of endobronchial ultrasound-guided transbronchial needle aspiration compared with mediastinoscopy for mediastinal lymph node staging of lung cancer. J Thorac Cardiovasc Surg 2011;142:1393-400.e1.
8. McLoud TC, Bourgouin PM, Greenberg RW, Kosiuk JP, Templeton PA, Shepard JA, Moore EH, Wain JC, Mathisen DJ, Grillo HC. Bronchogenic carcinoma: analysis of staging in the mediastinum with CT by correlative lymph node mapping and sampling. Radiology 1992;182:319-23.
9. Silvestri GA, Gonzalez AV, Jantz MA, Margolis ML, Gould MK, Tanoue LT, Harris LJ, Detterbeck FC. Methods for staging non-small cell lung cancer: Diagnosis

and management of lung cancer, 3rd ed: American College of Chest Physicians evidence-based clinical practice guidelines. Chest 2013;143:e211S-50S.
10. Schröder W, Baldus SE, Mönig SP, Beckurts TK, Dienes HP, Hölscher AH. Lymph node staging of esophageal squamous cell carcinoma in patients with and without neoadjuvant radiochemotherapy: histomorphologic analysis. World J Surg 2002;26:584-7.
11. Foley KG, Christian A, Fielding P, Lewis WG, Roberts SA. Accuracy of contemporary oesophageal cancer lymph node staging with radiological-pathological correlation. Clin Radiol 2017;72:693.e1-7.
12. Nagano H, Takumi K, Nakajo M, Fukukura Y, Kumagae Y, Jinguji M, Tani A, Yoshiura T. Dual-Energy CT-Derived Electron Density for Diagnosing Metastatic Mediastinal Lymph Nodes in Non-Small Cell Lung Cancer: Comparison With Conventional CT and FDG PET/CT Findings. AJR Am J Roentgenol 2022;218:66-74.
13. Gao L, Lu X, Wen Q, Hou Y. Added value of spectral parameters for the assessment of lymph node metastasis of lung cancer with dual-layer spectral detector computed tomography. Quant Imaging Med Surg 2021;11:2622-33.
14. Fukuya T, Honda H, Hayashi T, Kaneko K, Tateshi Y, Ro T, Maehara Y, Tanaka M, Tsuneyoshi M, Masuda K. Lymph-node metastases: efficacy for detection with helical CT in patients with gastric cancer. Radiology 1995;197:705-11.
15. Kirchner J, Broll M, Müller P, Pomjanski N, Biesterfeld S, Liermann D, Kickuth R. CT differentiation of enlarged mediastinal lymph node due to anthracosis from metastatic lymphadenopathy: a comparative study proven by endobronchial US-guided transbronchial needle aspiration. Diagn Interv Radiol 2015;21:128-33.
16. Volterrani L, Mazzei MA, Banchi B, Voltolini L, La Sala F, Carbone SF, Ricci V, Gotti G, Zompatori M. MSCT multi-criteria: a novel approach in assessment of mediastinal lymph node metastases in non-small cell lung cancer. Eur J Radiol 2011;79:459-66.
17. Hunt BM, Vallières E, Buduhan G, Aye R, Louie B. Sarcoidosis as a benign cause of lymphadenopathy in cancer patients. Am J Surg 2009;197:629-32; discussion 632.
18. Baldwin DR, Lambert L, Pantin CF, Prowse K, Cole RB. Silicosis presenting as bilateral hilar lymphadenopathy. Thorax 1996;51:1165-7.
19. Belperio JA, Shaikh F, Abtin FG, Fishbein MC, Weigt SS, Saggar R, Lynch JP 3rd. Diagnosis and Treatment of Pulmonary Sarcoidosis: A Review. JAMA 2022;327:856-67.
20. Kirchner J, Kirchner EM, Goltz JP, Obermann A, Kickuth R. Enlarged hilar and mediastinal lymph nodes in chronic obstructive pulmonary disease. J Med Imaging Radiat Oncol 2010;54:333-8.
21. Bilici A, Erdem T, Boysan SN, Acbay O, Oz B, Besirli K, Gundogdu S. A case of anthracosis presenting with mediastinal lymph nodes mimicking tuberculous lymphadenitis or malignancy. Eur J Intern Med 2003;14:444-6.
22. Kirchner J, Mueller P, Broll M, Kirchner EM, Pomjanski N, Liermann D, Biesterfeld S, Kickuth R. Chest CT findings in EBUS-TBNA-proven anthracosis in enlarged mediastinal lymph nodes. Rofo 2014;186:1122-6.
23. Bayanati H, E Thornhill R, Souza CA, Sethi-Virmani V, Gupta A, Maziak D, Amjadi K, Dennie C. Quantitative CT texture and shape analysis: can it differentiate benign and malignant mediastinal lymph nodes in patients with primary lung cancer? Eur Radiol 2015;25:480-7.

Cite this article as: Wang ZL, Yan Y, Li XT, Li YL, Li ZW, Sun YS. Usefulness of attenuation value on computed tomography plain scan for diagnosing enlarged mediastinal lymph nodes metastases. Quant Imaging Med Surg 2023;13(9):5759-5769. doi: 10.21037/qims-22-1305

Supplementary

Table S1 Pearson's r between CT features

Pearson's r	Long-axis diameter	Short-axis diameter	Short-axis/ long-axis ratio	Plain CT attenuation	Contrast-enhanced CT attenuation
Long-axis diameter	1	0.893*	–0.064	–0.223	–0.141
Short-axis diameter	0.893*	1	0.355*	–0.21	–0.099
Short-axis/long-axis ratio	–0.064	0.355*	1	–0.048	0.067
Plain CT attenuation	–0.223	–0.21	-0.048	1	0.439*
Contrast-enhanced CT attenuation	–0.141	–0.099	0.067	0.439*	1

*, P<0.05. CT, computed tomography.

https://dx.doi.org/10.21037/qims-22-1305